SUPRAMOLECULAR ORGANIC SEMICONDUCTING MATERIALS FOR OPTOELECTRONICS

Acronim: SUPRAMOL-MAT

Scientific Report STAGE 3 / 2024

Code project: PN-III-P4-PCE-2021-0906

PCE 120* din *14/06/2022

PROJECT MANAGER
Dr. Aurica Farcas

TEAM MEMBERS
1. Dr. Ana-Maria Resmerita
2. Dr. Ursu Laura-Elena
3. Dr. Balan-Porcărașu Mihaela
4. Dr. Asăndulesa Mihai
5. Dr. Tigoianu Ionut Radu
6. Dr. Peptu Cristian

Objectives/2024

W3.2. The synthesis of thiophene-phenylene-azomethine (TPA) and its inclusion complexes TPA/TMS·βCD,TPA/TMS·γCD,TPA/TMe·βCD, TPA/TMe·γCD and TPA/CB7;

W3.3. The synthesis of polyrotaxanes (PFTPA PRs) and the reference copolymer (PFTPA): Structural characterizations and photophysics by FTIR, NMR, GPC, TGA,

DSC, ESI-MS, UV-Vis, RAMAN and TEM;

W3.4. Electrochemical and morphological properties of PFTPA PRs and PFTPA;

W3.5. Electrical conductivities of PFTPA PRs and PFTA in their undoped and doped forms;

W3.6. Surface pressure-area isotherms and BAM studies of PFTPA PRs and PFTPA at the air/water interface;

W3.7. The testing in organic electronic devices: photovoltaics (PSCs) and other organic electronic devices

W3.2. - 2024

The synthesis of thiophene-phenylene-azomethine (**3**) and its inclusion complex **3·TMe-βCD**

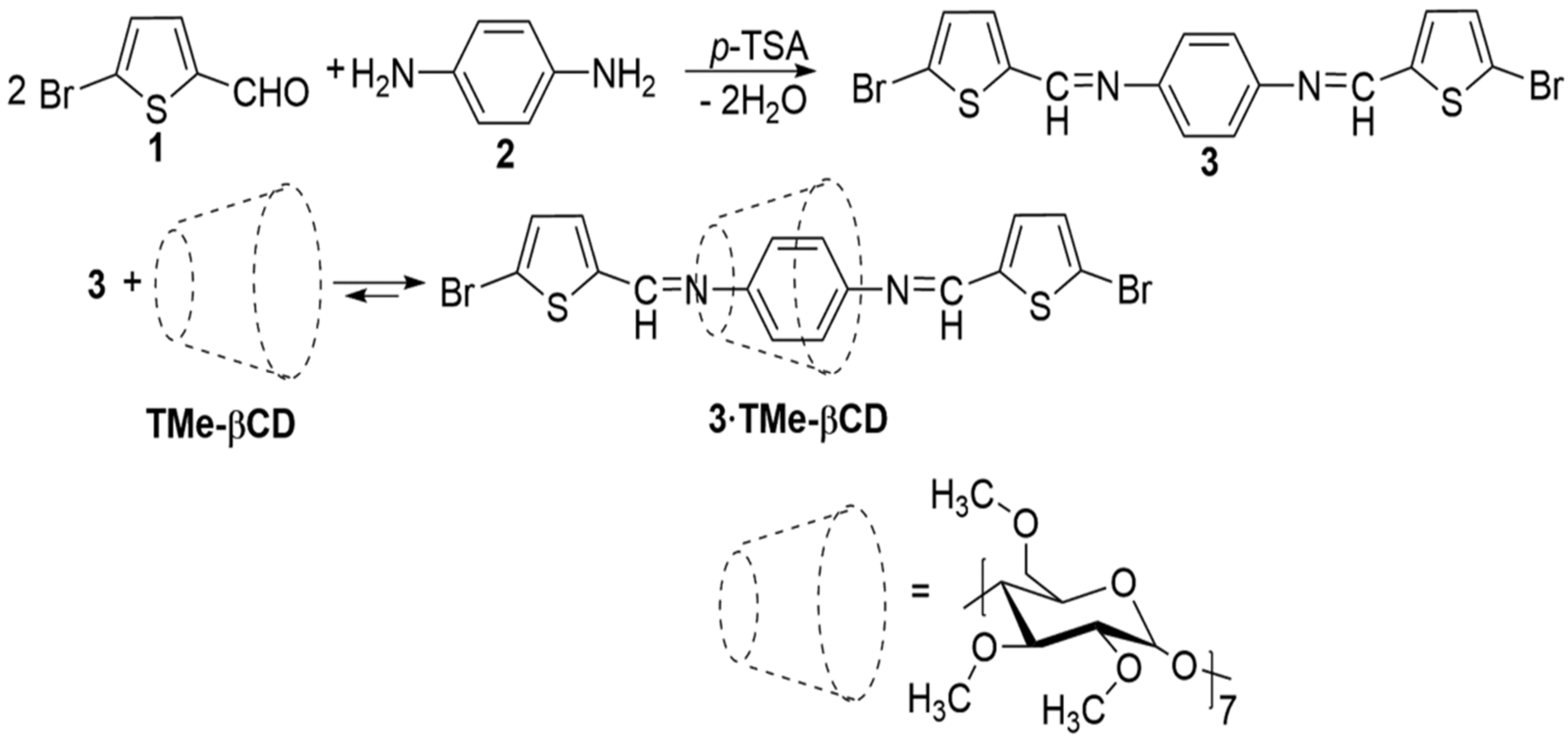

Scheme 1. Synthetic route to the target bisazomethine 3 and its encapsulated form 3·TMe-βCD.

Structural characterization

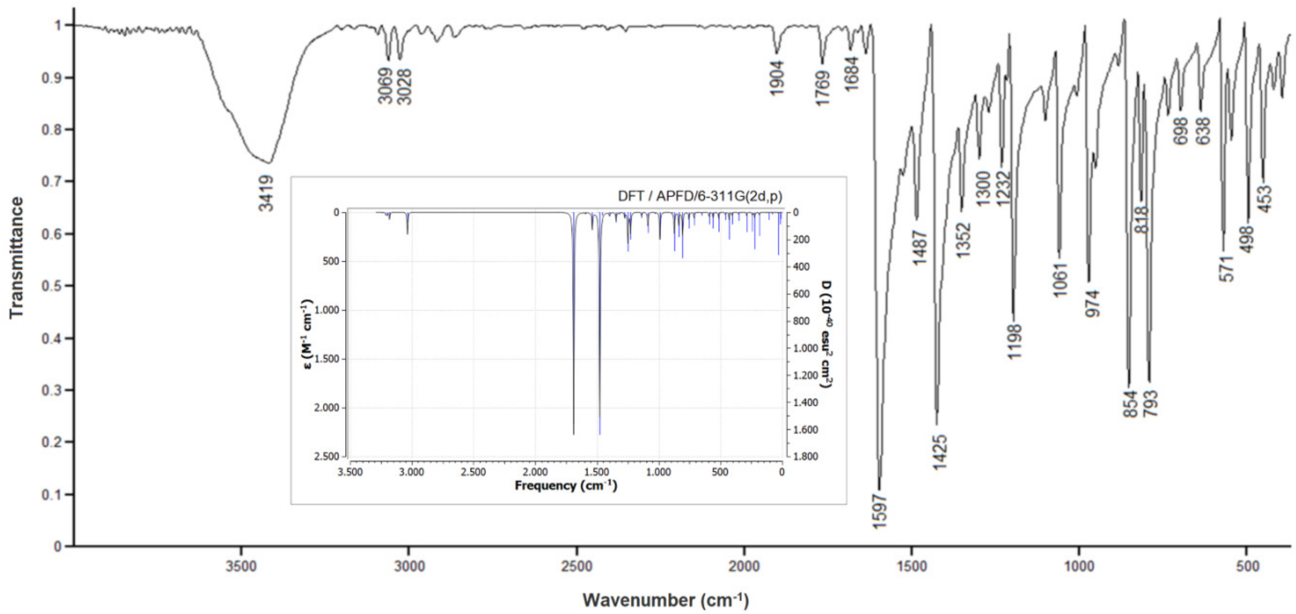

Figure 1. FT-IR spectrum correlated with DFT calculations of **3** bisazomethine.

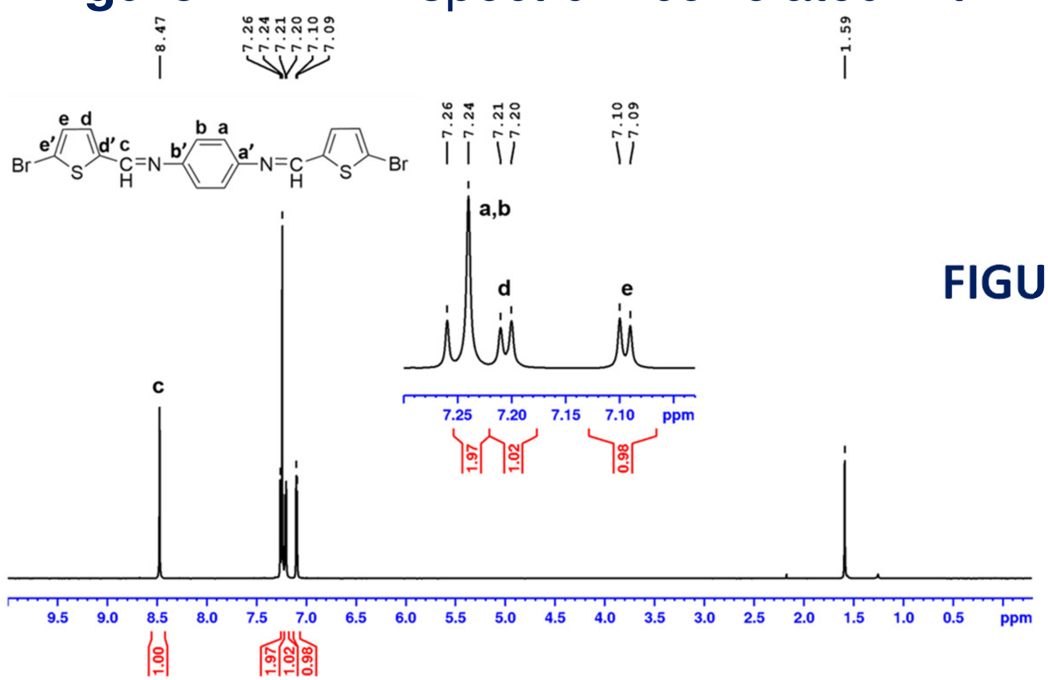

FIGURE 2. 1H-NMR spectrum of **3** in CDCl3.

The host-guest complexation stoichiometry

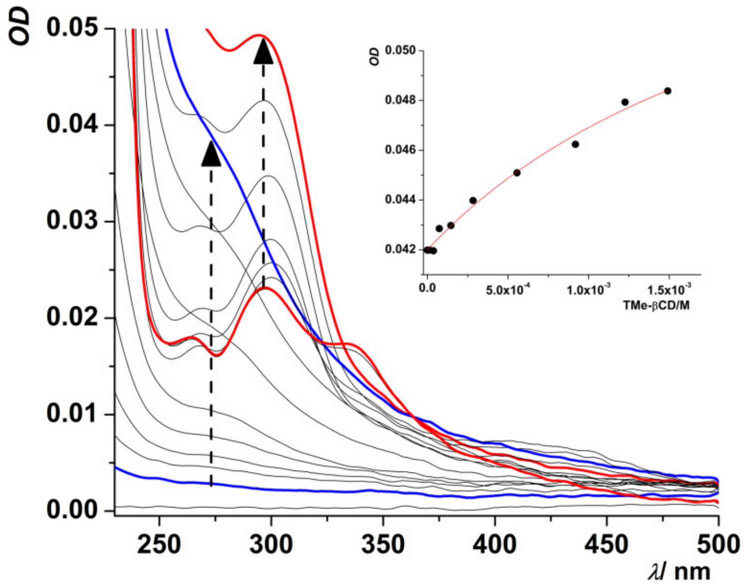

Figure 3. UV-Vis absorption titration of bisazomethine **3** monomer (1 μM solution in DCM) with increasing the concentration of TMe-βCD. The nonlinear fitting based on the UV-Vis absorption change assuming a 1:1 binding model, from which the association constant was derived.

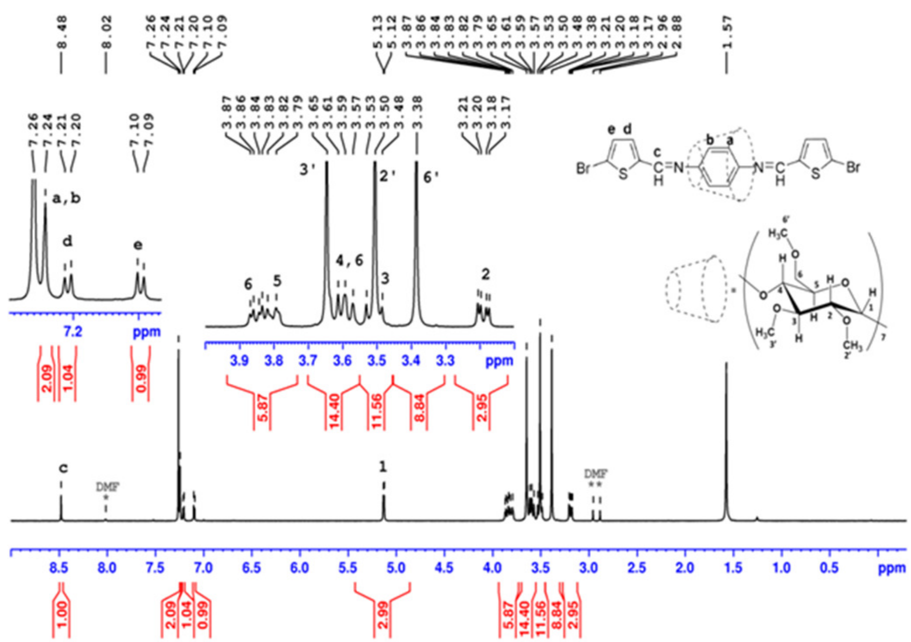

Figure 4. 1H-NMR spectrum of **3·TMe-βCD** in CDCl3.

DFT computations for exploring electronic structure

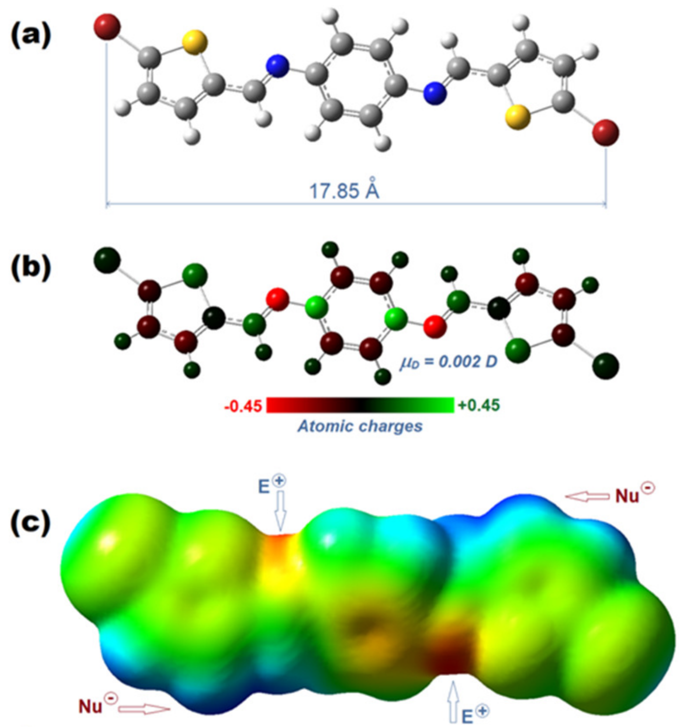

Figure 5. Molecular insights of compound **3**: Optimized geometry (conformation) by DFT method (a); distribution of partial atomic charges (Mulliken) and dipole moment value (b); electrostatic potential (c), represented as a mapped surface surrounding molecule 3, highlighting electrophilic attack sites (E+) and nucleophilic attack sites (Nu−); computation conducted at the APFD/6-311G(2d,p) theory level.

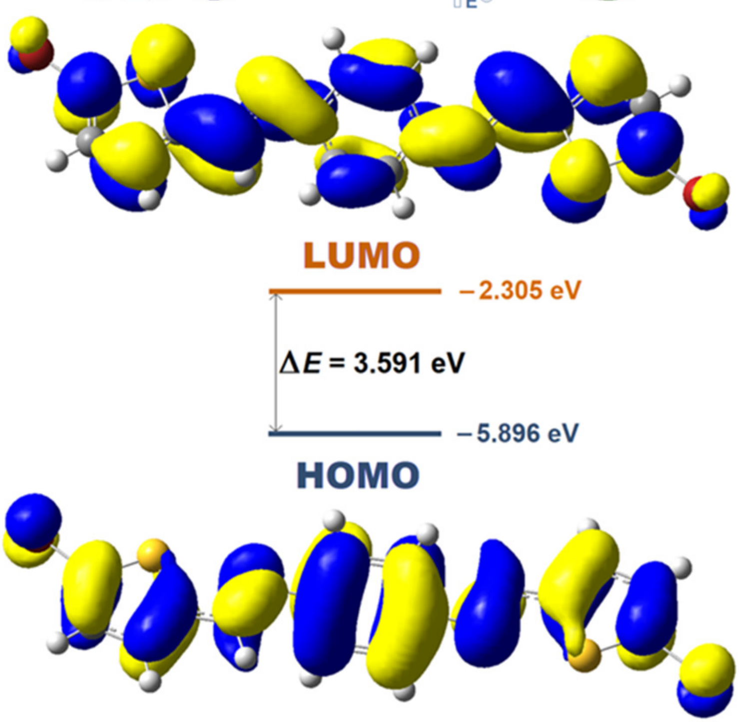

Figure 6. Frontier molecular orbital patterns (HOMO & LUMO) and corresponding band-gap energy value for compound **3**.

Molecular docking simulation

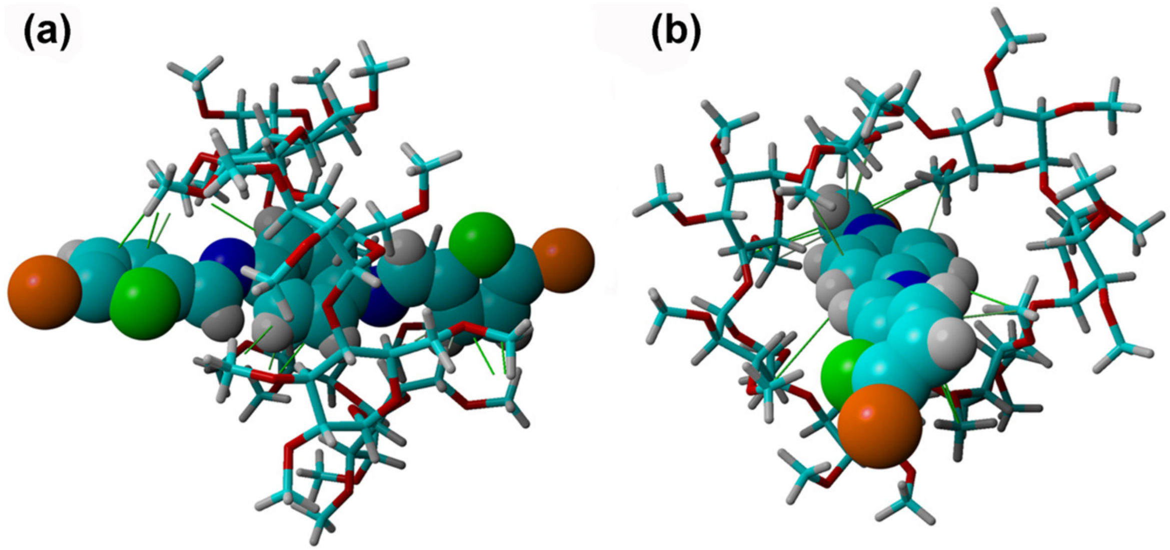

Figure 7. Molecular docking model of the best pose demonstrating inclusion complex formation between TMe-βCD (host) and molecule **3** (guest): (a) Side view of the **3·TMe-βCD** complex and (b) Top view of the **3·TMe-βCD** complex. Solid green lines are hydrophobic contacts.

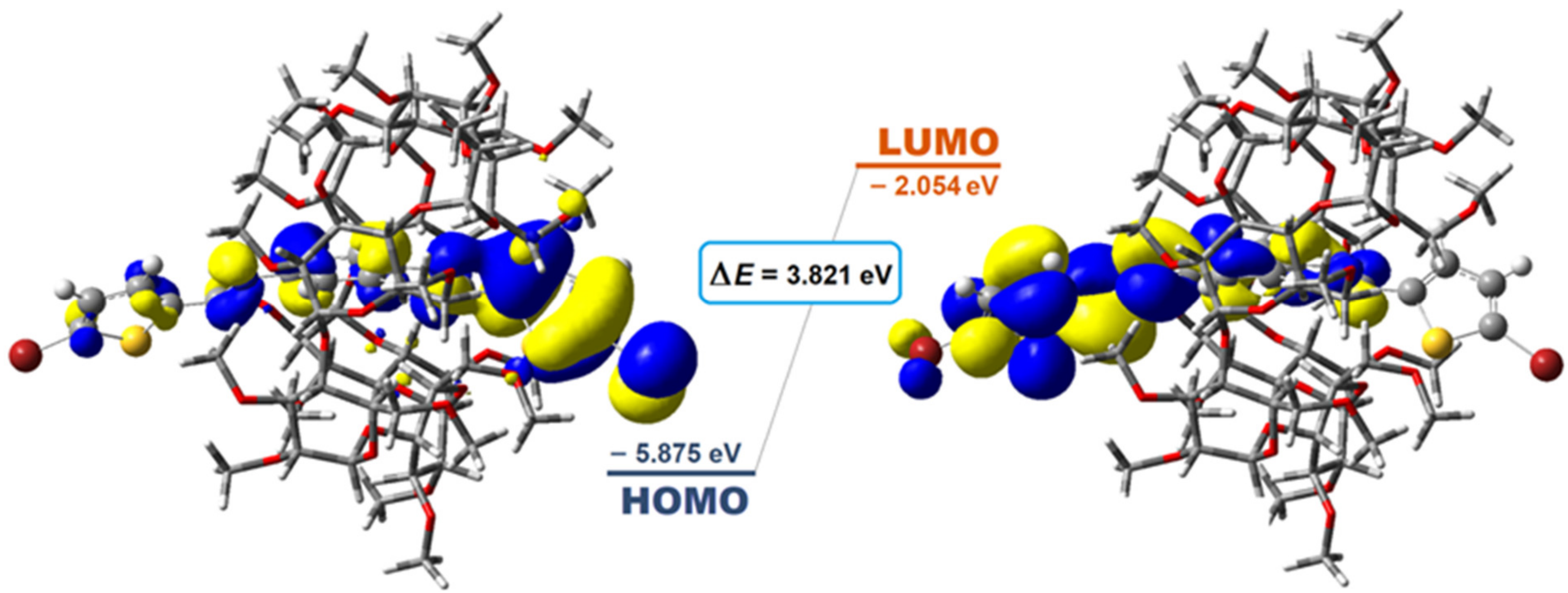

Figure 8. Frontier molecular orbital patterns (HOMO and LUMO) and corresponding band-gap energy value for the host-guest complex **3·TMe-βCD.**

The surface morphology

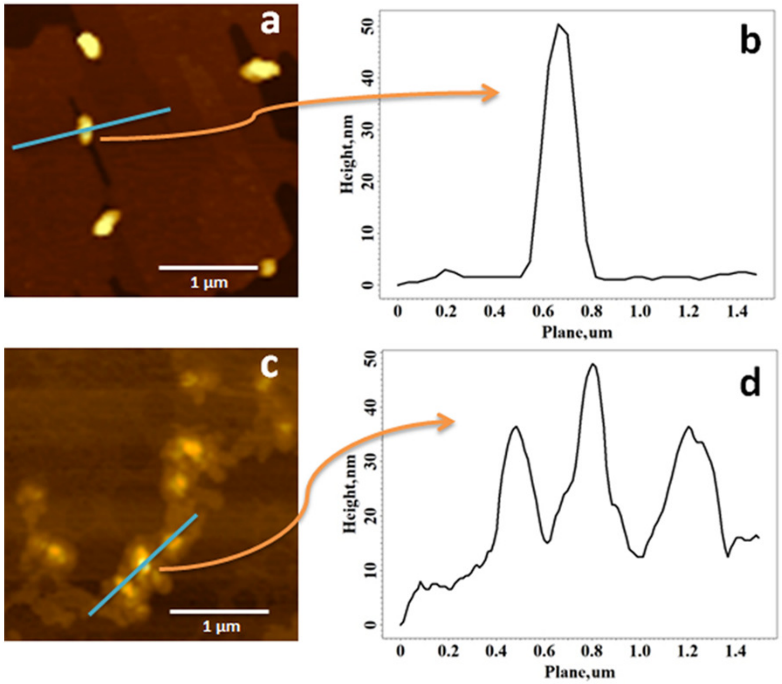

Figure 9. AFM images of **3** (a,b) and **3·TMe-βCD** (c,d) thin films prepared by drop-casting from THF solution.

Electrochemical properties

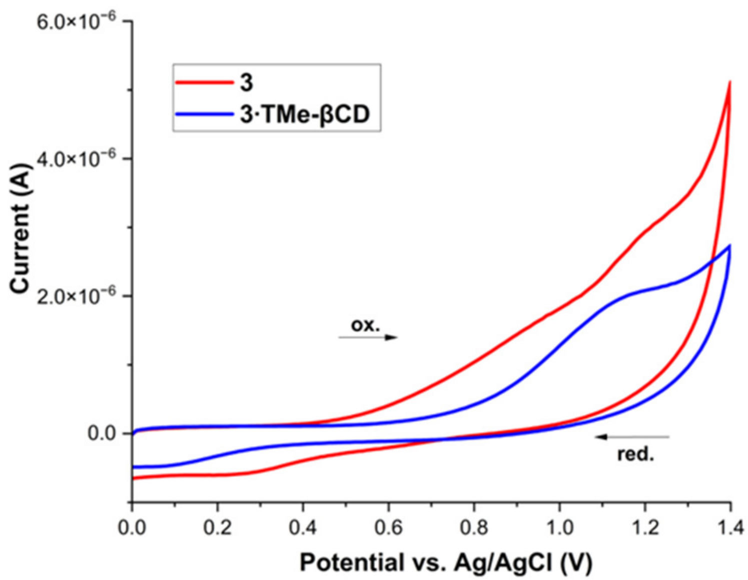

Figure 10. CV curves of **3** (red) and **3·TMe-βCD** (blue) in the anodic region, registered at 50 mV·s-1.

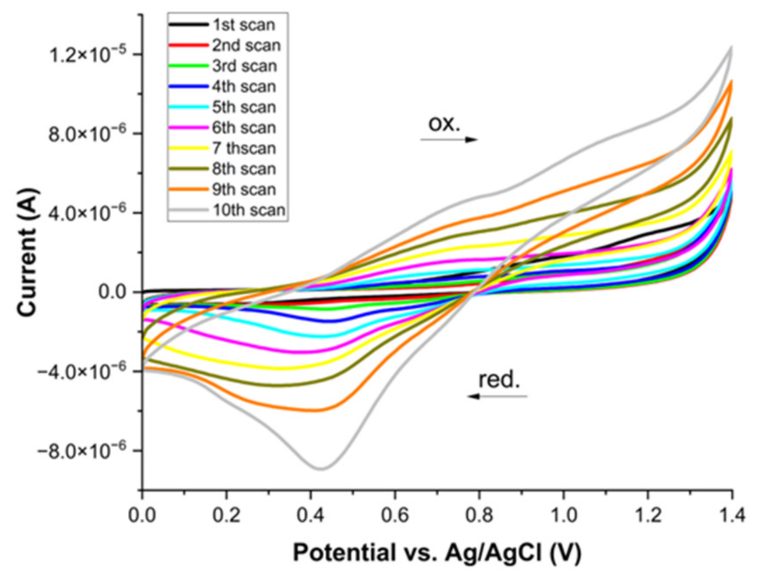

Figure 11. Repetitive 10 CV scans of 3 in the anodic region registered at 50 mV·s-1.

Surface pressure-area isotherms and BAM studies of 3 and 3·TMe-βCD monolayers

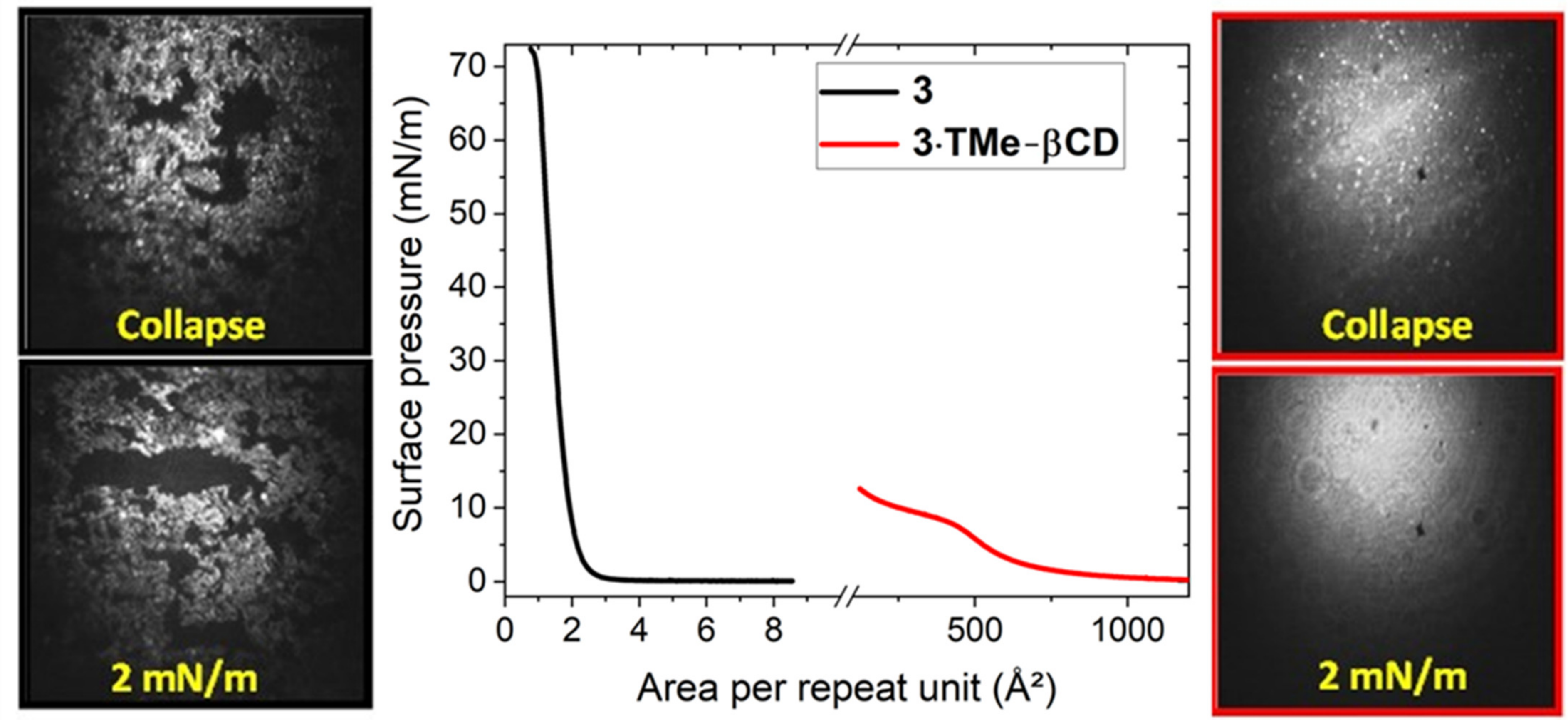

Figure 12. Compression isotherms and BAM images (600 µm x 600 µm) of **3** (black frame) and **3·TMe-βCD** (red frame) monolayers at 2 mN·m-1 and in the collapsed phases.

W3.3. Sinteza polirotaxanilor si a polimerului de referinta

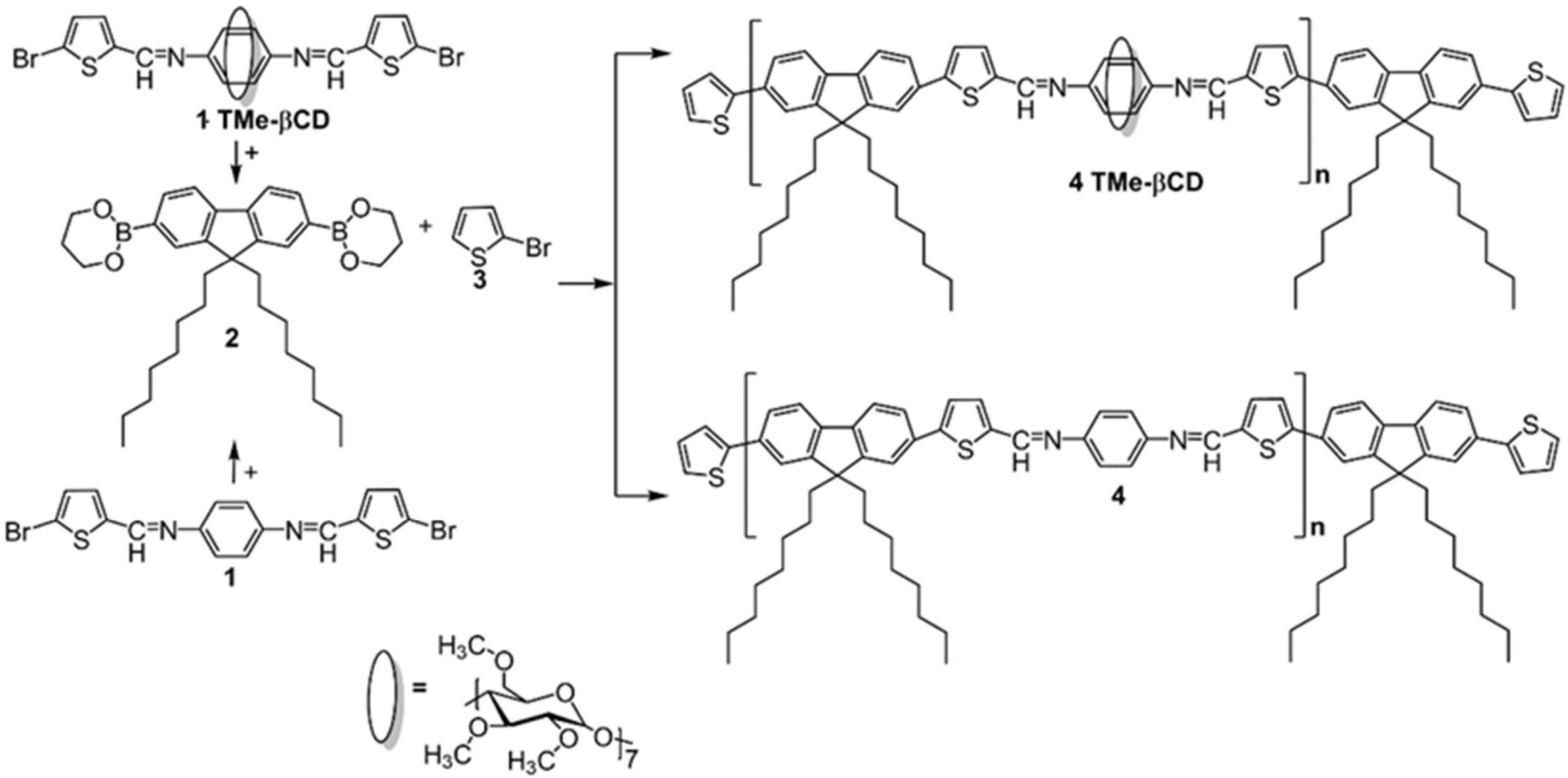

Scheme 2. Synthesis protocol of **4·TMe-βCD** and **4** bisazomethine-based copolymers.

Structural characterizations

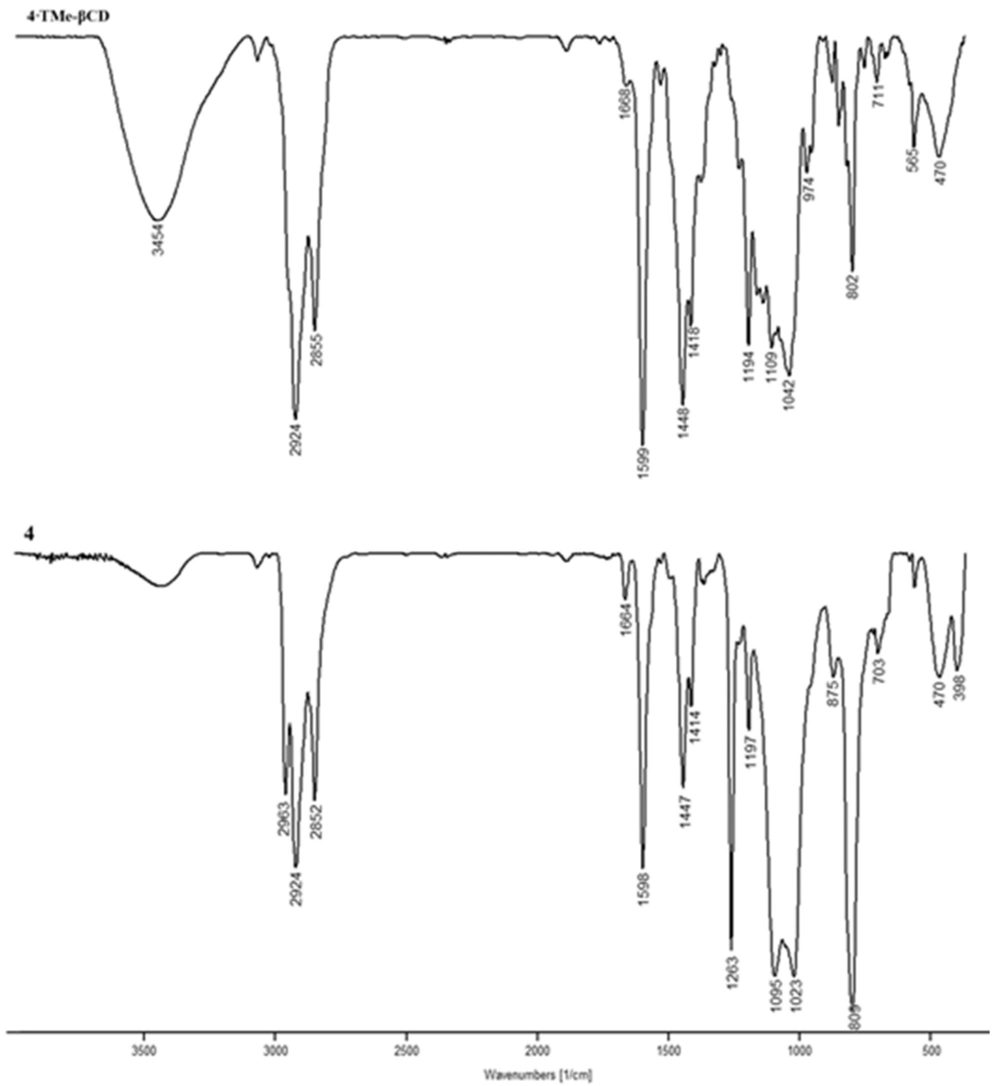

Figure 13. FT-IR spectra of **4·TMe-βCD** and **4**.

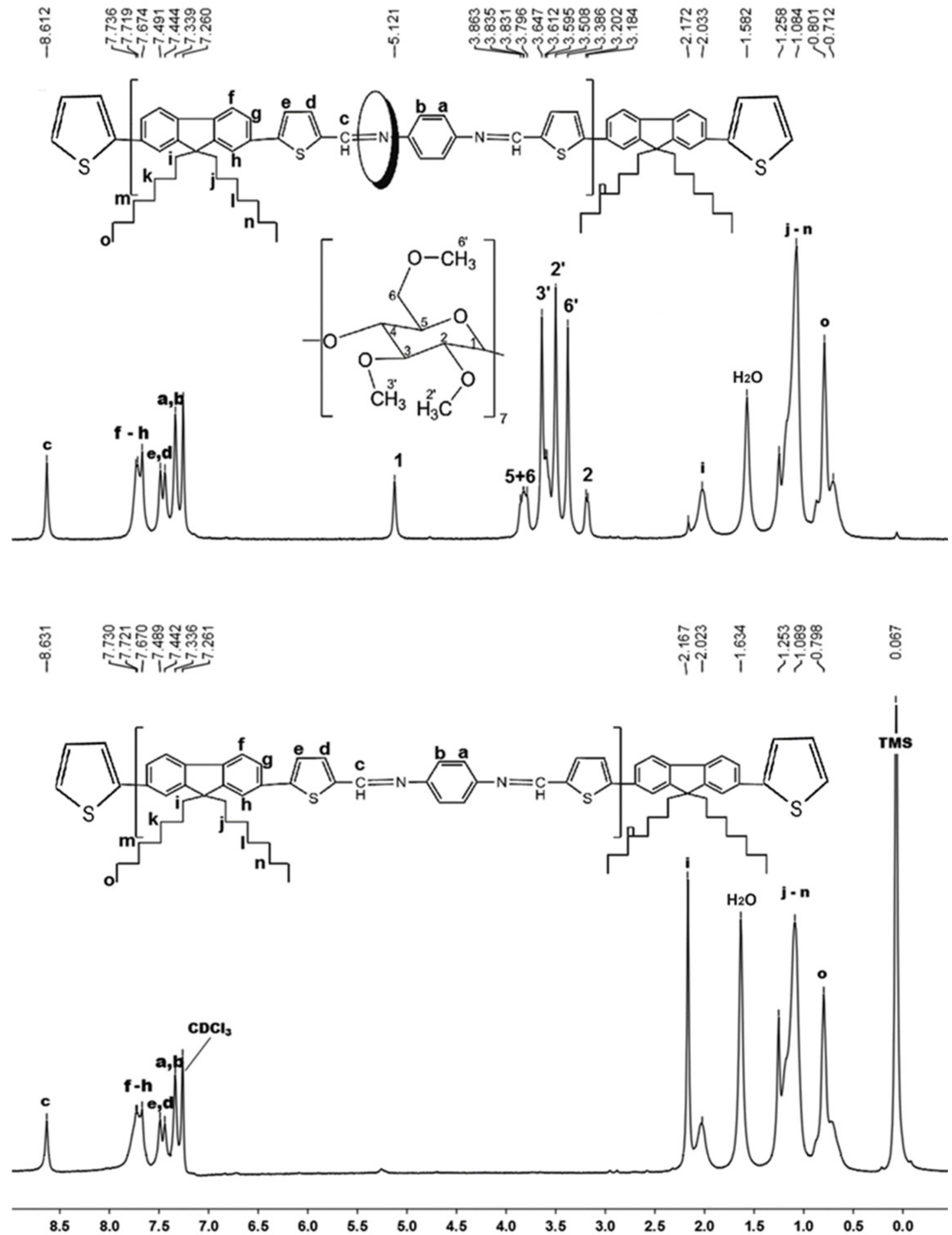

Figure 14. 1H-NMR spectra of the 4·TMe-βCD (top) and 4 (bottom) in CDCl3.

The surface morphology

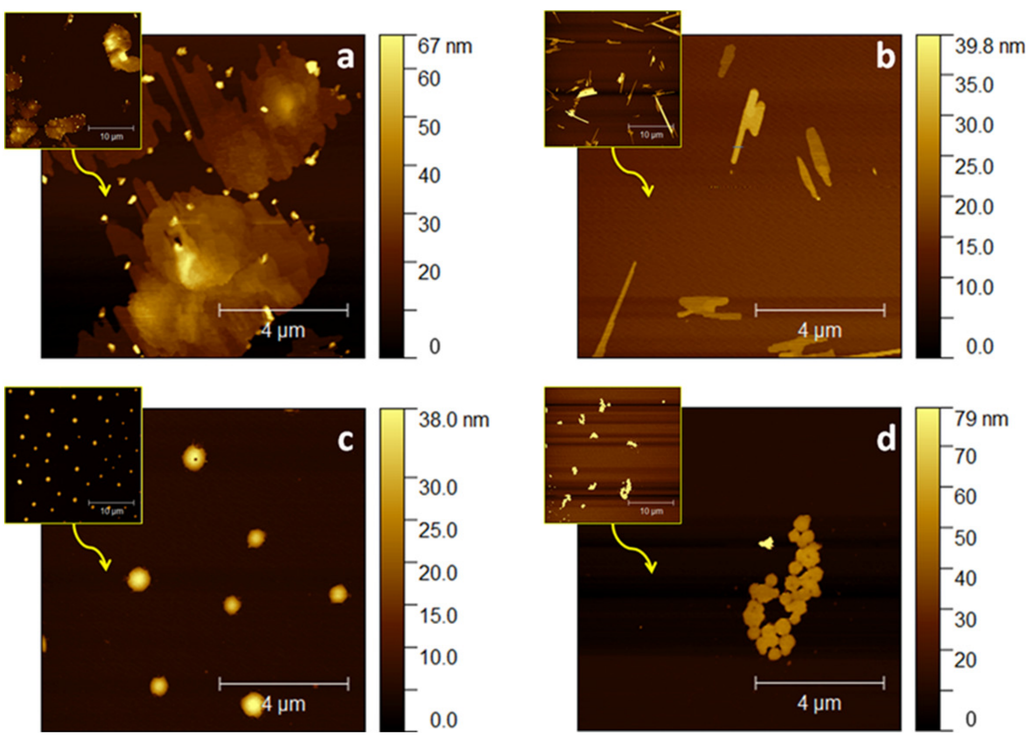

Figure 15. AFM images of **1** (a,b) and **4** (c,d) thin films prepared by drop-casting from THF solution in concentrated and dilute regimes, respectively.

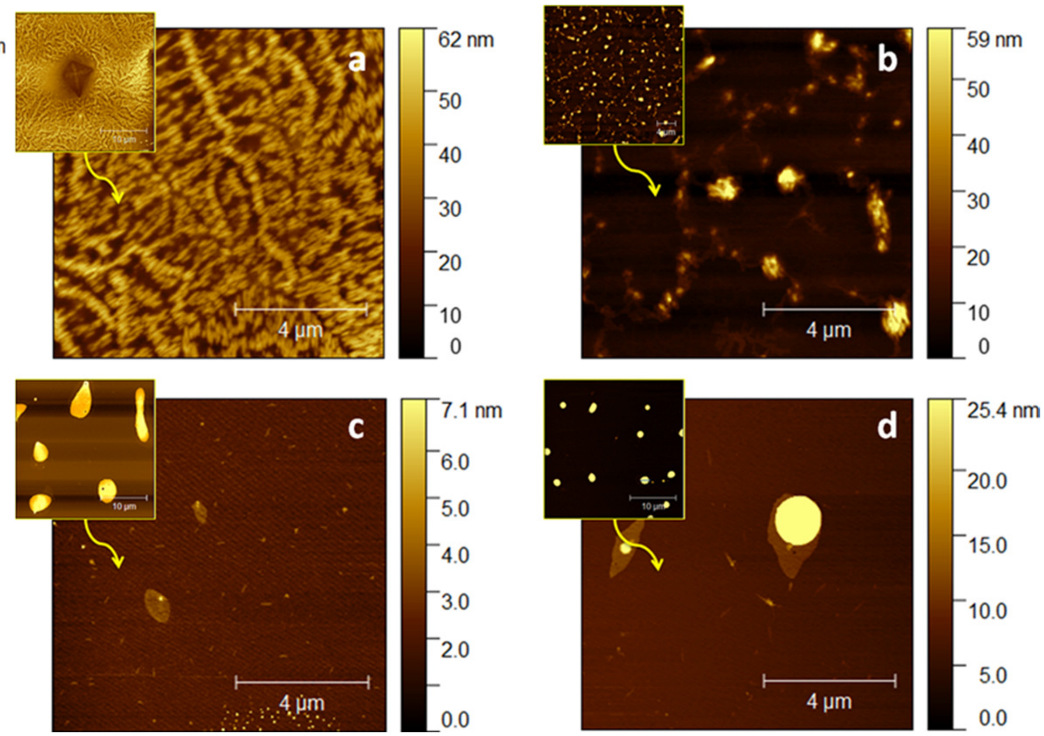

Figure 16. AFM images of **1·TMe-βCD** (a,b) and **4·TMe-βCD** (c,d) thin films prepared by drop-casting from THF solution in concentrated and dilute regime, respectively.

Optical Properties

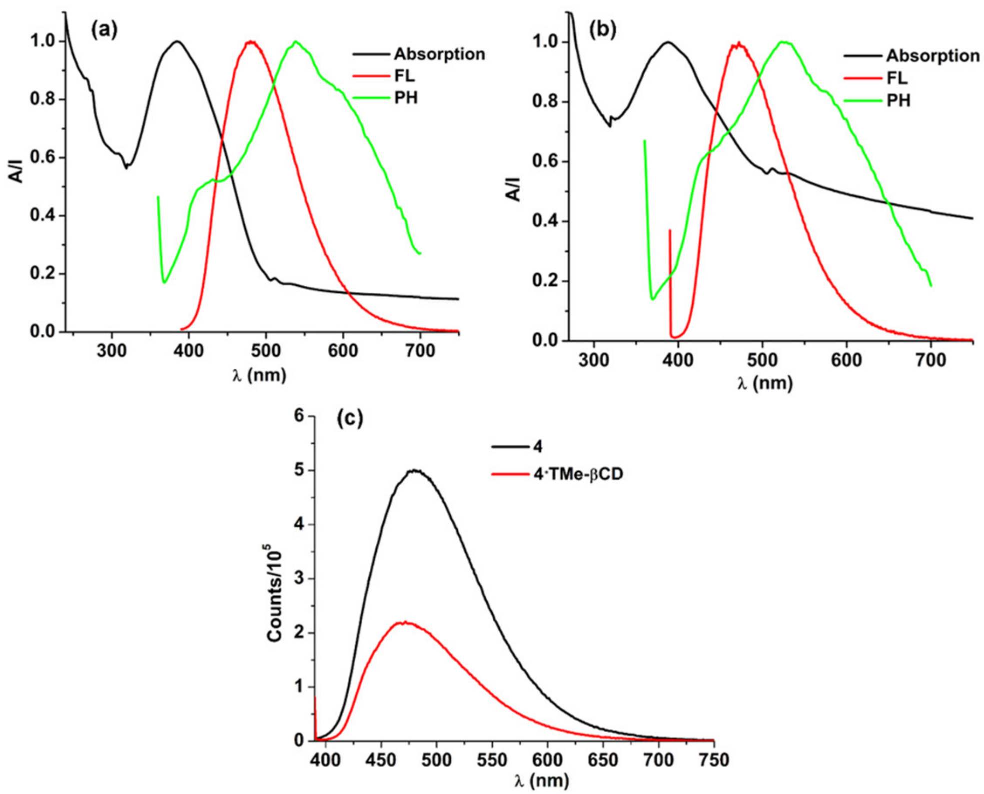

Figure 17. UV-Vis absorption, fluorescence and phosphorescence spectra of **4** (a) and **4·TMe-βCD** (b) and fluorescence spectra of **4** and **4·TMe-βCD** (c) at λex = 375.

Sample	λ_{ex} (nm)	λ_{em} (nm)	τ_1 (ns)	τ_2 (ns)	Φ_{FL} (%)	Φ_{Ph} (%)
4	375	483	1024.37(62.92%)	8743.53(37.08%)	13.41	11.75
4·TMe-βCD	“	472	1126.55(67.67%)	9275.79(32.33%)	22.03	46.76

Table 1. Emission lifetimes (τ) and chi-squared (χ2) determined by nanosecond transient absorption, and quantum yields for fluorescence (ΦFL) and phosphorescence (ΦPh) of the synthesized Schiff bases **4** and **4·TMe-βCD** in ACN.

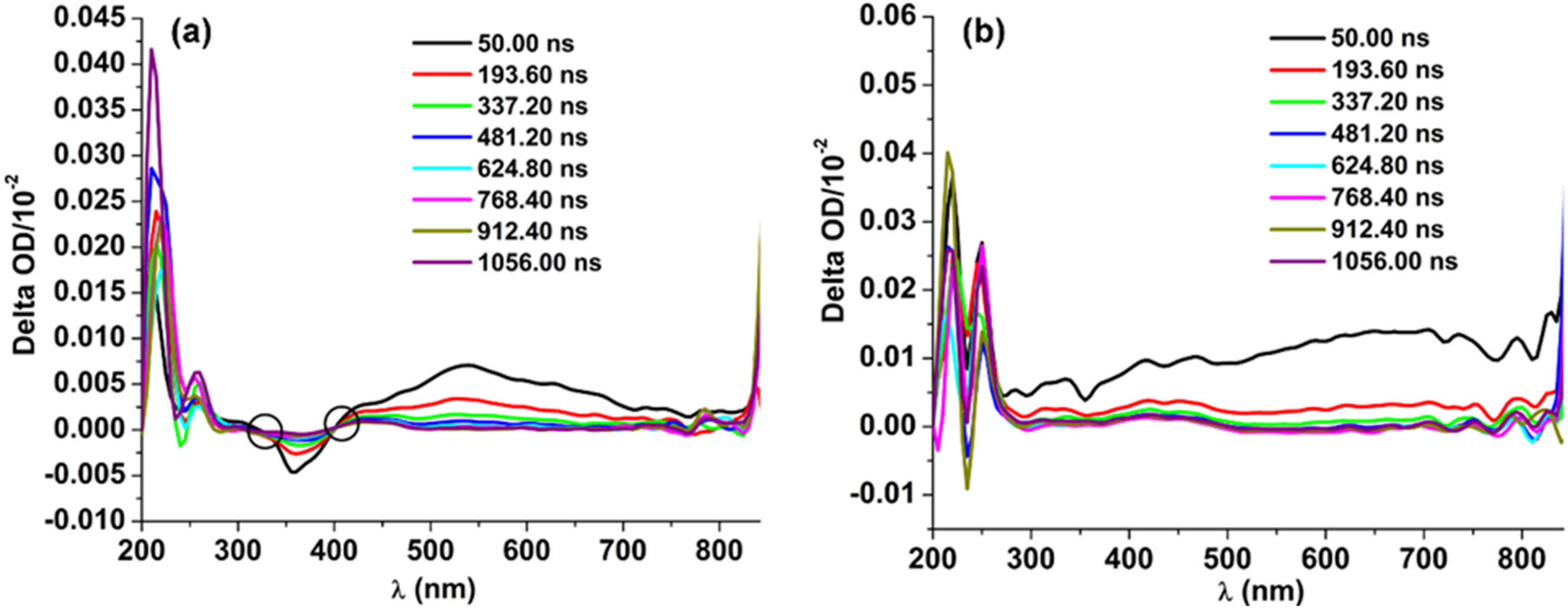

Figure 18. Nanosecond transient absorption maps of **4** (a) and **4·TMe-βCD** (b) in ACN (λex = 375 nm) (the black circle shows the isosbestic points).

Electrochemical properties

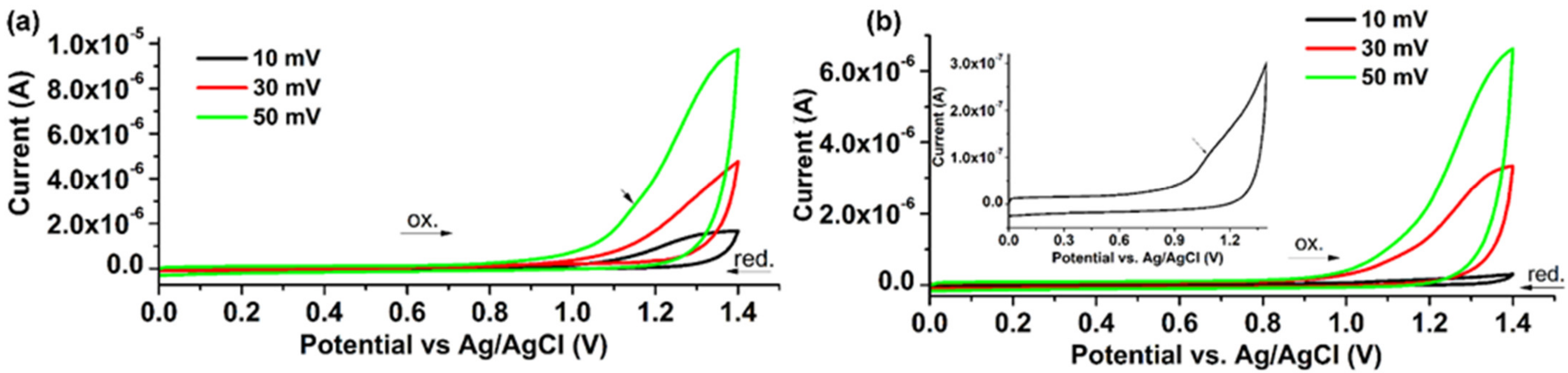

Figure 19. Cyclic voltammograms of fresh films of **4** (a) and **4·TMe-βCD** (b) at different scan rates, in the anodic region (inset: enlarged view of the CV curve of **4·TMe-βCD** at 10 mV·s-1).

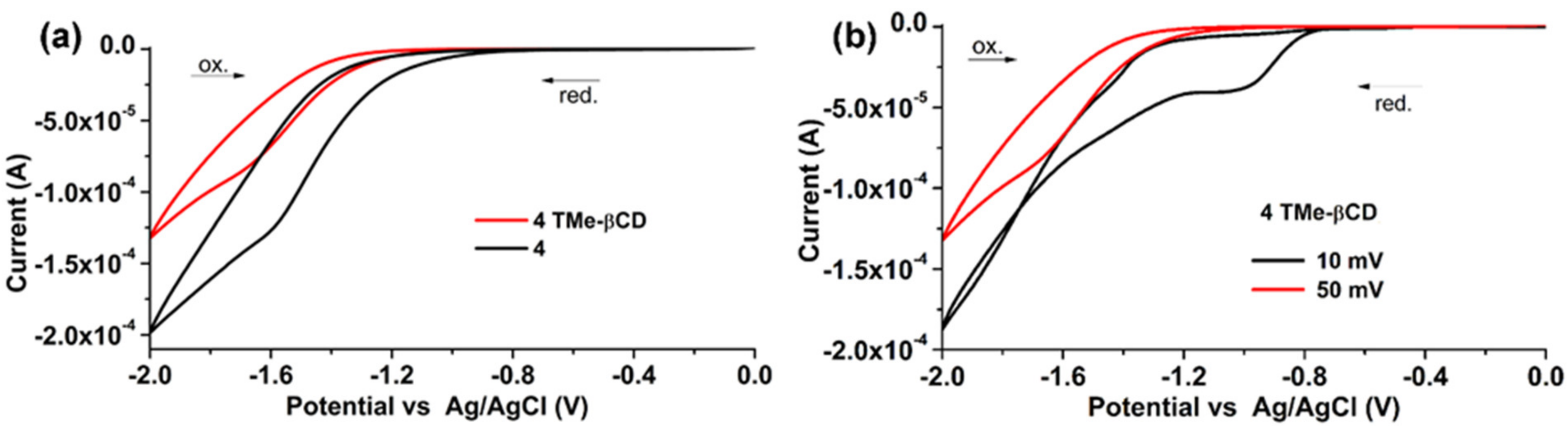

Figure 20. Cyclic voltammograms of **4** and **4·TMe-βCD** at 50 mV·s-1 (left) and comparative CV curves of **4·TMe-βCD** at 10 and 50 mV·s-1 (right) in the cathodic region.

Electrical properties

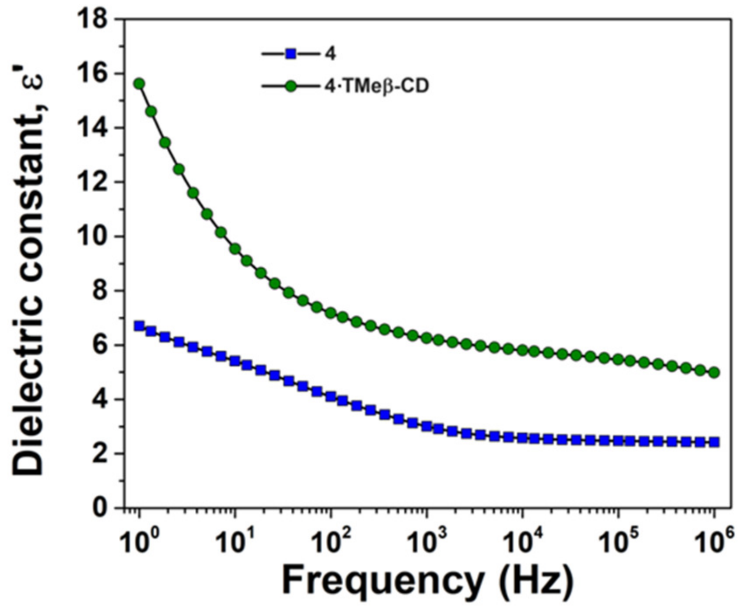

Figure 21. Variation of dielectric constant as a function of frequency of **4** and **4·TMe-βCD**.

Table 2. Electrical conductivities of **4** and **4·TMe-βCD**.

Sample	σ ($S \cdot cm^{-1}$)[a)]	σ ($S \cdot cm^{-1}$)[b)]	σ ($S \cdot cm^{-1}$)[c)]
4	2.1×10^{-11}	7.3×10^{-10}	8.5×10^{-7}
4·TMe-βCD	6.2×10^{-12}	8.1×10^{-11}	2.2×10^{-8}

a)Conductivity measured by BDS method of undoped pellets; b)Conductivity measured by the four-point method of undoped pellets; c) Conductivity measured by the four-point method of iodine-doped pellets.

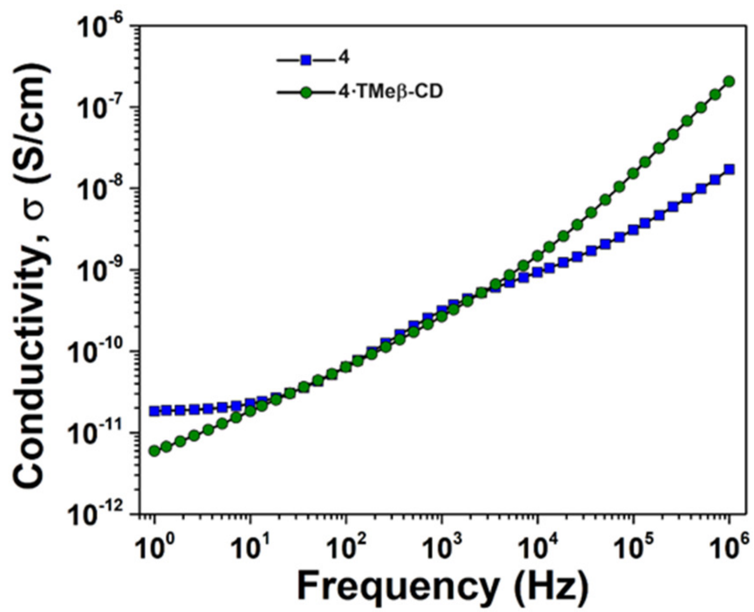

Figure 22. The variation of σ with f under alternating electrical field of **4** and **4·TMe-βCD** samples.

Surface pressure-area isotherms and BAM studies of Langmuir monolayers

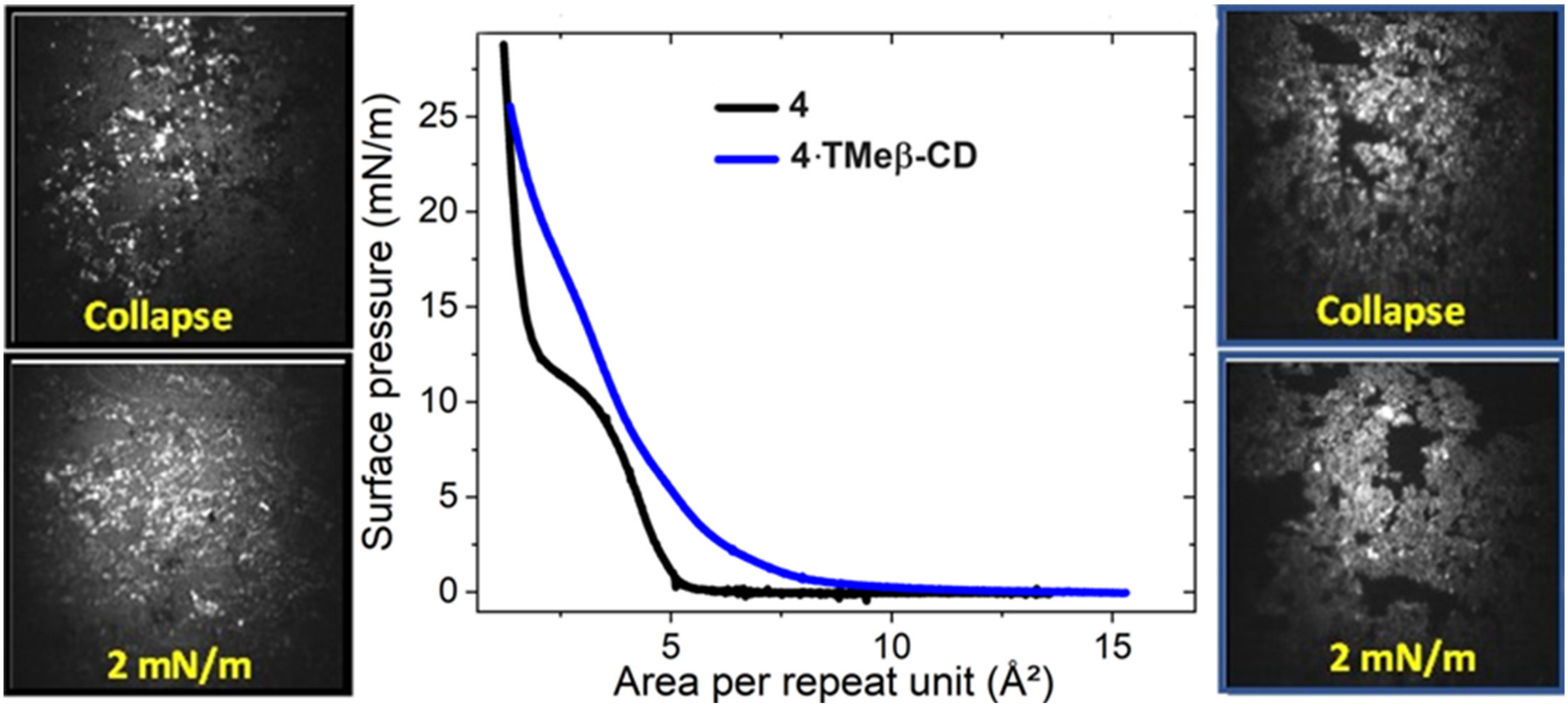

Figure 23. Compression isotherms and BAM images (600 µm x 600 µm) of **4** (black frame) and **4·TMe-βCD** (blue frame) monolayers at 2 mN·m-1 and in the collapsed phases.

Diode fabrication

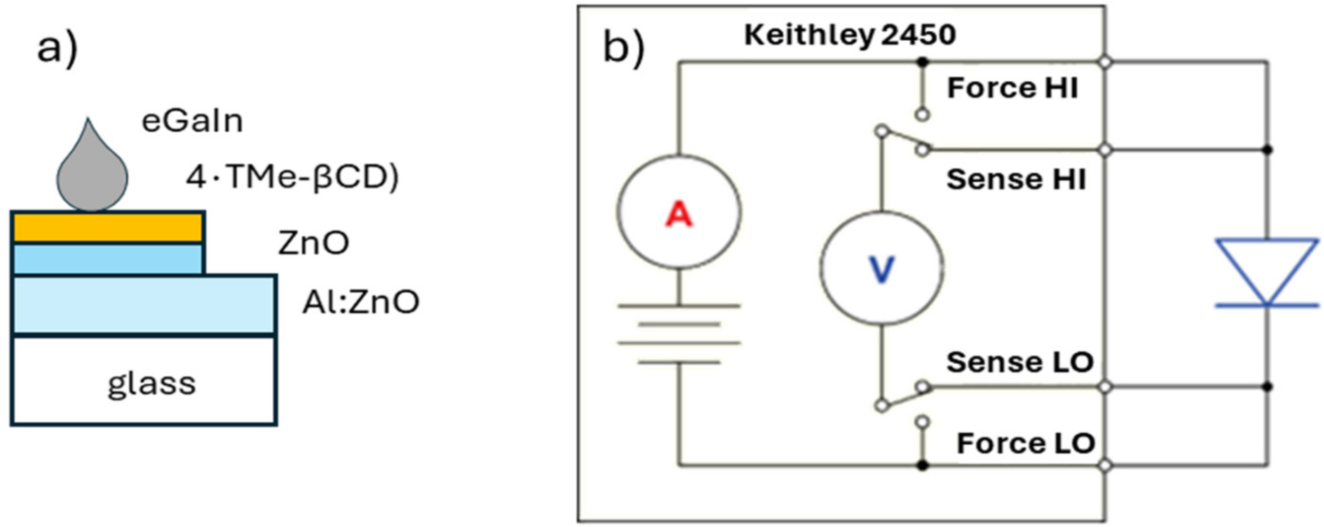

Manufactured prototype diode structure (a) and schematic diagram used to connect the source measurement unit to the diode in a 4-wire configuration (b).

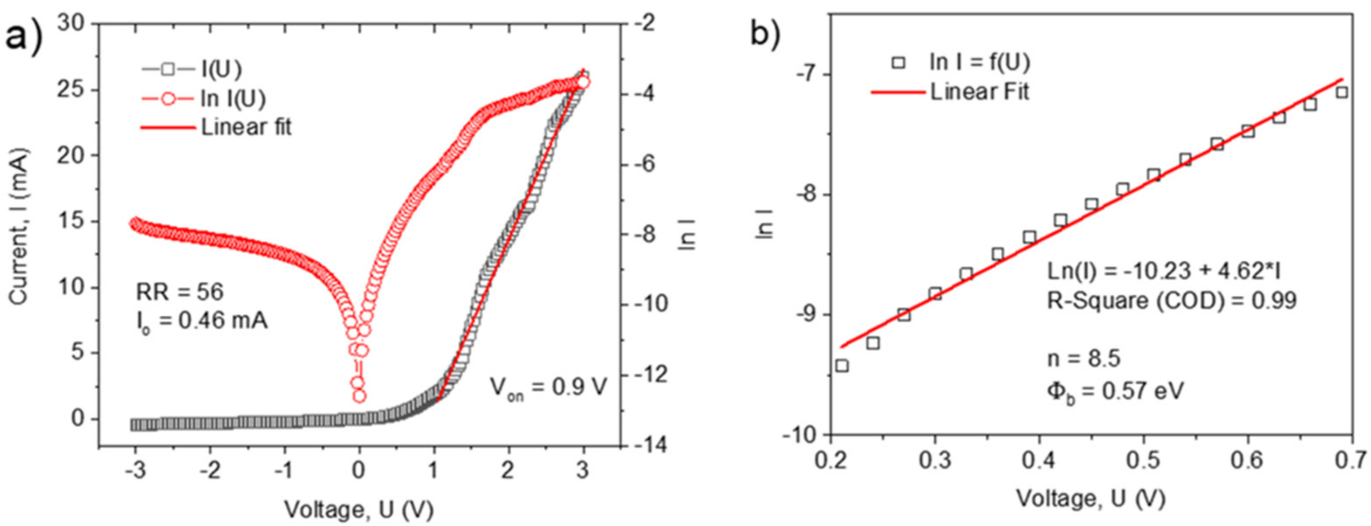

This value is quite close to conventional diodes and similar to the reported values for hybrid diodes found in the literature

Measured current-voltage characteristic of the eGaIn/4TMe-βCD/ZnO/Al:ZnO manufactured diode: a) the nonlinear current-voltage characteristic I=f(U); and b) the representation of the linear region from the semilogarithmic plot.

Preliminarily photovoltaic results of 4·TMeβCD and 4

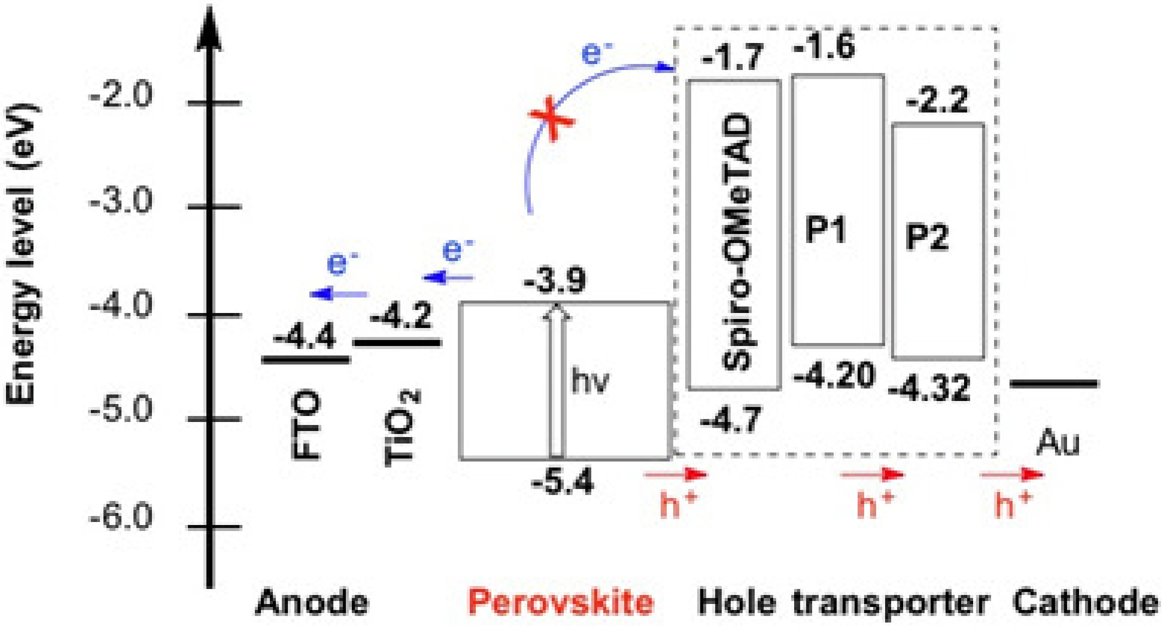

Figure 23. Energy level alignment of different device components.

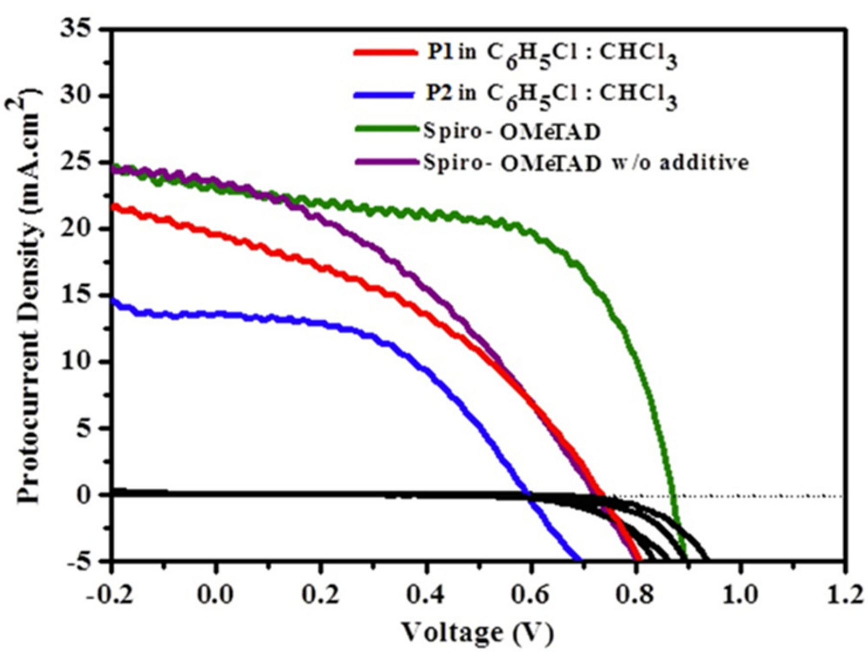

Figure 24. J-V curves of **P1** (**4·TMeβCD**-red) and **P2** (**4**-blue).

Dissemination - 2024

ISI published papers: 3

1. B. Hajduk , P. Jarka, H. Bednarski , H. Janeczek , P. Kumari , A. Farcas
Thermal transitions and structural characteristics of poly(3,4-ethylenedioxythiophene/cucurbit[7]uril) polypseudorotaxane and polyrotaxane thin films,
Materials 2024, 17, 1318. https://doi.org/10.3390/ma17061318

2. A.-M. Resmeriţă, M. Asăndulesa, A. Farcaş, Composite materials based on slide-ring polyrotaxane structures for optoelectronics ,
J. Polym. Sci. 2024, 1-11. https://doi.org/10.1002/pol.20240285

3. A.-M. Resmerita, C. Cojocaru, M.-D. Damaceanua, M. Balan-Porcarasu, S. Shova, A. El Haitami, A. Farcas
A thiophene-based bisazomethine and its inclusion complex with permethylated β-cyclodextrin: Exploring structural characteristics and computational chemistry models,
Dyes Pigm. 2024, 232, 112472. https://doi.org/10.1016/j.dyepig.2024.112472

4. C. Ursu, A.-M. Resmerita, R. I. Tigoianu, A. Farcas
Aromatic co-polyazomethine polyrotaxane with enhanced solubility applied as a hole carrier in a p-n heterojunction diode,
ACS Appl. Polym. Mater. 2024. ap-2024-03090t- accepted

Plenary conferences: 3

1. A. Farcaş, Supramolecular encapsulation of semiconductors as a promising approach to organic electronic materials, Semiconductor Materials Forum -SEMICONFORUM2024, 11-15 august/2024, Madrid-Spania.
https://www.continuumforums.com/2024/semiconforum

2. A. Farcaş, A.-M. Resmeriţă, SUPRAMOLECULAR SEMICONDUCTORS TOWARD ORGANIC ELECTRONIC MATERIALS, PolyChar World Forum on Advanced Materials
30th Edition, September 11 - 13, 2024, Iasi -Romania

3. A. Farcaş, SUPRAMOLECULAR ORGANIC SEMICONDUCTORS: RECENT ADVANCES AND PERSPECTIVES FOR OPTOELECTRONICS, CNCHIM2024 NATIONAL CONFERENCE OF CHEMISTRY. XXXVII EDITION, September 25-27, 2024,Targoviste-Romania

4. A. Farcaș, Semiconducting interlocked molecular architectures toward organic (bio)electronics, LPPI, CY Cergy Paris Université F95000 Cergy, France, 09.10.2024 (Conferinta invitata)

Other:

1. A. Farcaş - Program Committee, KEYNOTE SPEAKER at the Semiconductor Materials Forum -SEMICONFORUM2024, 11-15 august/2024, Madrid-Spania. https://www.continuumforums.com/2024/semiconforum
2. Chair for the Semiconductors and Optoelectronics Forum (SEMICONFORUM 2024), 12-14 august 2024, Madrid-Spain
3. Apreciere asupra activității de promovare a chimiei în România, Diploma de Onoare acordată de Societatea de Chimie din România (SChR), 25 septembrie 2024.